

# Self-Purification Mitigates Backdoors in Multimodal Diffusion Language Models

Guangnian Wan, Qi Li, Gongfan Fang, Xinyin Ma, Xinchao Wang\*  
 National University of Singapore  
 guangnian@u.nus.edu, xinchao@nus.edu.sg

## Abstract

*Multimodal Diffusion Language Models (MDLMs) have recently emerged as a competitive alternative to their autoregressive counterparts. Yet their vulnerability to backdoor attacks remains largely unexplored. In this work, we show that well-established data-poisoning pipelines can successfully implant backdoors into MDLMs, enabling attackers to manipulate model behavior via specific triggers while maintaining normal performance on clean inputs. However, defense strategies effective to these models are yet to emerge. To bridge this gap, we introduce a backdoor defense framework for MDLMs named DiSP (Diffusion Self-Purification). DiSP is driven by a key observation: selectively masking certain vision tokens at inference time can neutralize a backdoored model’s trigger-induced behaviors and restore normal functionality. Building on this, we purify the poisoned dataset using the compromised model itself, then fine-tune the model on the purified data to recover it to a clean one. Given such a specific design, DiSP can remove backdoors without requiring any auxiliary models or clean reference data. Extensive experiments demonstrate that our approach effectively mitigates backdoor effects, reducing the attack success rate (ASR) from over 90% to typically under 5%, while maintaining model performance on benign tasks. Code is available [here](#).*

## 1. Introduction

Multimodal Large Language Models (MLLMs) [18, 23, 35, 49] have demonstrated remarkable performance across a wide range of tasks [6, 12, 58, 66]. While most existing MLLMs are built upon autoregressive (AR) large language models (LLMs), an emerging line of research explores discrete diffusion language models as a promising alternative. Unlike AR-based MLLMs that generate text in a fixed left-to-right manner, Multimodal Diffusion Language Models (MDLMs) produce text through an iterative denoising process, progressively refining an initially masked token se-

quence into a coherent sequence of text tokens. Benefiting from this design, MDLMs offer the potential for faster inference and more flexible generation control [59, 60].

The growing promise of MDLMs naturally raises concerns about their trustworthiness in real-world applications [20, 25, 26, 50]. In this work, we present the first analysis of MDLMs under backdoor attacks from both attack and defense perspectives. This attack surface is of broad practical significance, especially in the era of large-scale models, where the possibility that costly models may behave abnormally when exposed to poisoned data is intolerable for developers [32, 34, 40]. An adversary could exploit this by uploading poisoned datasets to fine-tuning-as-a-service platforms [1, 17] or releasing them publicly, causing downstream users to unknowingly compromise their models. For MDLMs, we empirically demonstrate that they remain highly vulnerable to backdoor attacks. Even a standard data poisoning pipeline originally designed for AR-based models can successfully implant backdoors in MDLMs. However, existing defense strategies cannot be directly transferred to MDLMs, leaving their protection against backdoor threats largely unaddressed. These findings highlight the urgent need for defenses specifically tailored to the unique characteristics of MDLMs.

To bridge this gap, we propose Diffusion Self-Purification (DiSP), a purification framework specially designed for backdoor defense in MDLMs. DiSP builds on our findings on MDLMs’ unique decoding mechanism: Benefiting from its training paradigm [27, 59], MDLMs can flexibly take partially masked inputs and generate the missing tokens in the masked positions. When such masked regions are placed in the visual part of the token embeddings, a model can still seamlessly handle such inputs on clean data, producing coherent and semantically appropriate text. In contrast, when applied to a backdoored model with poisoned data, selectively masking certain visual embeddings can suppress the trigger-induced behavior and cause the model’s outputs to revert to their clean, untriggered form.

Leveraging this property, given a model compromised by training on a poisoned dataset, we run inference on these training data under the masked-input prompting scheme that

---

\*Corresponding author.

selectively masks a subset of image tokens. This inference regime neutralizes trigger-driven behaviors and yields a purified set of input–output pairs. We then fine-tune the model on this purified dataset to remove the embedded backdoor. Notably, unlike common ‘filter-then-finetune’ pipelines that discard trigger-containing samples and fine-tune on what remains [45], DiSP retains those inputs and rewrites their responses into the untriggered form before fine-tuning. In our experiments, explicitly including triggered inputs paired with purified responses in the fine-tuning data leads to more effective backdoor removal than re-training solely on the dataset’s original clean subset.

Within this framework, the central challenge lies in determining which tokens should be masked. To this end, we estimate the saliency of each visual token as the local directional curvature of the output KL-divergence at the first generation step with respect to perturbations of the input embeddings. Tokens with the highest saliency values are subsequently masked. The rationale behind this design is that if a model’s behavior is strongly driven by a specific input pattern (trigger), the MDLM will exhibit high confidence in generating the trigger-induced response from the very beginning of the generation process. Such an early predictive distribution is dominated by tokens most sensitive to the trigger pattern. By masking these dominant tokens, we interrupt the information flow that activates the trigger pathway and thus enable the model to produce clean responses even when the trigger is present. For clean inputs, masking these tokens does not substantially affect the model’s predictions, which allows the subsequently fine-tuned model to maintain its performance without noticeable degradation.

We position our contributions as the first exploration of backdoor threats in Multimodal Diffusion Language Models (MDLMs). We demonstrate that MDLMs are still vulnerable to backdoor attacks and introduce DiSP, a tailored framework that leverages their distinctive generative behaviors for effective defense. Extensive experiments conducted on two representative MDLMs, covering diverse backdoor targets and various trigger patterns, validate both their susceptibility to backdoor attacks and the strong effectiveness of our proposed defense.

## 2. Related Work

### 2.1. Multimodal Diffusion Language Models

MLLMs have demonstrated strong performance across diverse vision-language tasks [3, 4, 18, 23, 35, 49]. Most MLLMs couple a pretrained LLM with a vision encoder (e.g., CLIP [43] or SigLIP [47, 65]) and a projector, extending the LLMs’ capabilities to visual understanding tasks [36]. Since mainstream LLMs adopt the AR paradigm, most MLLMs are likewise AR-based [2, 24]. Recently, diffusion language models (DLMs) have emerged as

an alternative paradigm for text generation [41, 57], which has in turn motivated the development of diffusion-based MLLMs. Representative MDLMs such as LLaDA-V [59], LaViDa [27], and Dimple [61] have demonstrated performance competitive with their AR-based counterparts.

### 2.2. Backdoor Attack

Backdoor attacks [8, 14] embed concealed malicious behaviors into models, causing normal outputs on clean inputs but attacker-controlled outputs when a trigger is present. Early work mainly focuses on unimodal models. Gu et al. [14] introduce this threat with BadNets, showing that a poisoned dataset can make models output attacker-specified labels when exposed to trigger patterns. Subsequent works extend this risk to encoder-only language models [22], image diffusion models [10, 11], and large language models [30, 44, 52, 53, 55]. Recent studies further extend backdoor attacks to multimodal settings, demonstrating their feasibility in CLIP-style architectures [5, 33, 56], and AR MLLMs [32, 40]. Despite this progress, the vulnerability of MDLMs remains largely unexplored.

### 2.3. Backdoor Defense

A wide range of defenses have been proposed to counter backdoor attacks [16, 29, 38, 42, 45, 54, 64], which can be broadly categorized into training-time defense and post-training methods. Training-time defenses aim to prevent backdoor implantation during model training. ABL [28] suppresses backdoor learning via sample isolation and gradient ascent on suspected backdoor examples, but is limited to classification tasks. BYE [45] detects anomalous samples through attention analysis and re-trains the model on the filtered dataset, but relies on AR generation. Post-training defenses seek to detect or mitigate backdoors in trained models without access to the training process. Neural Cleanse [48] detects and reconstructs triggers through reverse engineering. SentiNet [9] localizes highly-salient regions to detect triggers. However, they are also limited to classification tasks. STRIP [13] perturbs inputs at inference and flags low-entropy outputs as backdoored, but depends on unimodal assumptions. Some methods use a reference model to filter overly confident tokens [31] or employ auxiliary models to disrupt trigger patterns [46]. Despite these advances, existing defenses are largely restricted to unimodal models, AR generation, or rely on auxiliary models or external clean data, leaving backdoor defense for MDLMs largely unaddressed.

## 3. Method

### 3.1. Threat Model

Following prior works [16, 45], we consider a data-poisoning backdoor threat model. The adversary may arbi-

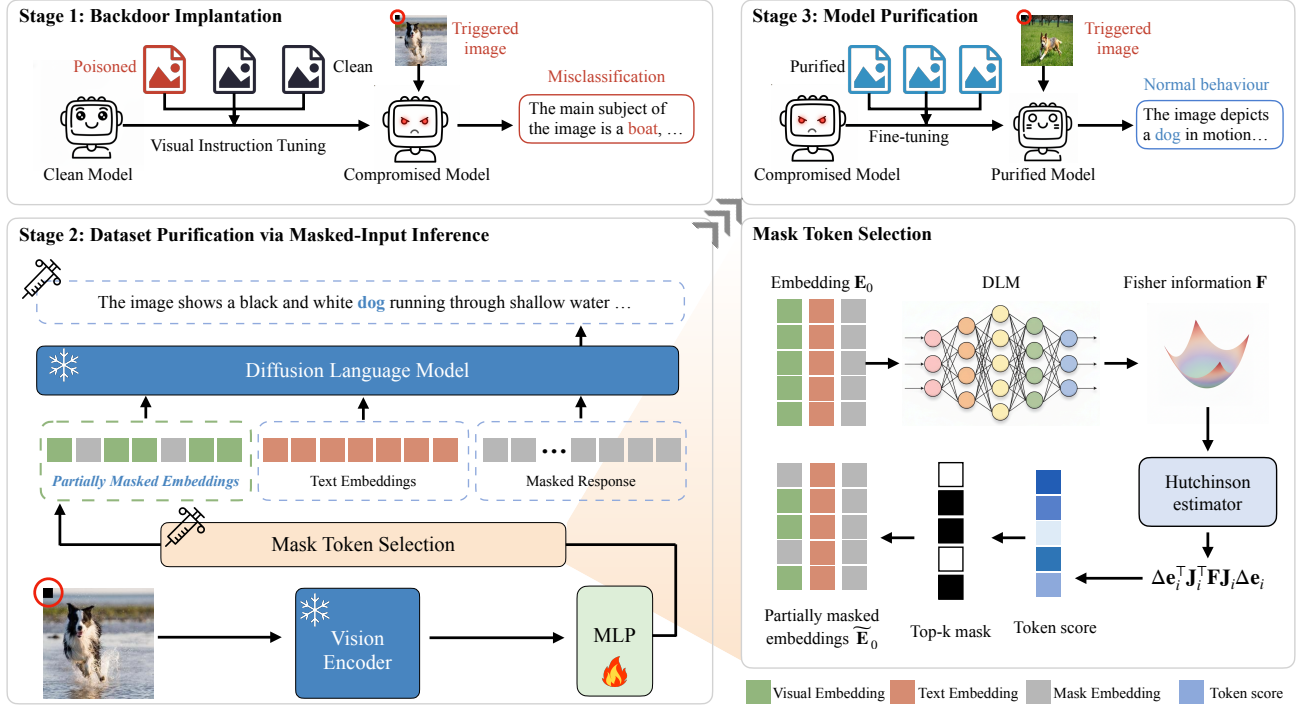


Figure 1. Overview of our proposed DiSP method.

trarily modify the training dataset, for example, by injecting a proportion of poisoned samples into an otherwise clean dataset, to control the behavior of the model trained on this data. However, the training procedure must follow existing visual instruction tuning methods, meaning that the adversary cannot alter other training components (e.g., training loss). For our defense, we assume that the defender has full control over the training process and has access to the complete training dataset, but possesses no prior knowledge about which samples are poisoned. The defender is also not required to use any additional clean reference data. This setting reflects practical scenarios in which users train models on third-party datasets that may not be fully trustworthy.

### 3.2. Backdoor Threats in MDLM

In a standard visual instruction tuning setting, each training example consists of an image  $v$ , a text prompt  $p$ , and a textual response  $x_0$ . We denote the clean training dataset as  $\mathcal{D}_{\text{clean}} = \{(v_i, p_i, x_{0,i})\}_{i=1}^N$ . To implant a backdoor, an adversary injects poisoned samples into the clean data. Each poisoned sample contains an image modified with a trigger, denoted by  $v^{\text{trig}}$ , and an attacker-specified response  $x_0^{\text{adv}}$ . We denote the poisoned set by  $\mathcal{D}_{\text{poison}} = \{(v_j^{\text{trig}}, p_j, x_{0,j}^{\text{adv}})\}_{j=1}^K$ . The training set used to train the compromised model is  $\mathcal{D}_{\text{train}} = \mathcal{D}_{\text{clean}} \cup \mathcal{D}_{\text{poison}}$ .

Unlike AR-based language models, discrete diffusion language models involve a forward masking process and

a reverse denoising process [59]. Given a clean sequence  $x_0 = (x_0^1, \dots, x_0^L)$  at  $t = 0$ , the forward process produces a partially masked sequence  $x_t$  by independently corrupting each position according to a time-dependent masking schedule. Let  $\alpha_t \in [0, 1]$  be the probability that a token remains unmasked at time  $t$ , with  $\alpha_0 = 1$ ,  $\alpha_1 = 0$ , and  $\alpha_t$  decrease decreases monotonically in  $t$ . The forward process can be written as Eq. 1:

$$q_{t|0}(x_t | x_0) = \prod_{i=1}^L q_{t|0}(x_t^i | x_0^i),$$

$$q_{t|0}(x_t^i | x_0^i) = \begin{cases} 1 - \alpha_t, & \text{if } x_t^i = [\text{MASK}], \\ \alpha_t, & \text{if } x_t^i = x_0^i, \\ 0, & \text{otherwise.} \end{cases} \quad (1)$$

A neural network parameterized by  $\theta$  is used to model the reverse process  $p_\theta(x_s | x_t)$ , where  $1 \geq t \geq s \geq 0$ . For each training instance, following the canonical training procedure [27, 41], we sample a diffusion timestep  $t \in [0, 1]$  and a partially masked target sequence  $x_t$  using the forward process in Eq. 1. The model is then trained to perform the reverse denoising process, modeled by the conditional distribution  $p_\theta(x_0 | v, p, x_t)$ . The training objective is formu-

---

**Algorithm 1** Diffusion Self-Purification (DiSP)
 

---

- 1: **Input:**  $\mathcal{D}_{\text{train}} = \mathcal{D}_{\text{clean}} \cup \mathcal{D}_{\text{poison}}$ , target MDLM  $M_\theta$ , mask ratio  $\rho$
  - 2: **Output:** purified dataset  $\tilde{\mathcal{D}}$ , purified MDLM  $\tilde{M}_\theta$
  - 3:  $M_\theta^{\text{back}} \leftarrow$  Fine-tune MDLM on  $\mathcal{D}_{\text{train}}$   $\triangleright$  Finetuning on poisoned dataset
  - 4: **for all**  $(v, p, x_0) \in \mathcal{D}_{\text{train}}$  **do**
  - 5:   compute  $\mathbf{p} \leftarrow \text{softmax}(f_{\theta_{\text{LM}}}(\mathbf{E}_0)[L_{\text{prompt}}+1:L_{\text{prompt}}+T, :])$   $\triangleright$  Predictive distribution
  - 6:    $\mathbf{F} \leftarrow \text{diag}(\mathbf{p}) - \mathbf{p}\mathbf{p}^\top$   $\triangleright$  Fisher information
  - 7:   draw  $\mathbf{q}^{(j)} \sim \mathcal{N}(\mathbf{0}, \mathbf{F})$  for  $j = 1 \dots m$   $\triangleright$  Hutchinson probe sampling
  - 8:    $s^{(j)} \leftarrow \langle \mathbf{q}^{(j)}, \text{vec}(\mathbf{L}_{\text{gen}}) \rangle$ ,  $\mathbf{g}^{(j)} \leftarrow \nabla_{\mathbf{E}_v} s^{(j)}$   $\triangleright$  Quadratic-form probe & backprop to visual embeddings
  - 9:    $\hat{s}_i \leftarrow \frac{1}{2m} \sum_{j=1}^m \langle \mathbf{g}_i^{(j)}, \Delta \mathbf{e}_i \rangle^2$   $\triangleright$  Visual-token score
  - 10:    $k = \lfloor \rho L_v \rfloor$ ,  $\mathcal{I}_{\text{mask}} = \text{Top-}k(\{\hat{s}_i\})$   $\triangleright$  Select tokens to mask
  - 11:   construct  $\mathbf{E}_v$  by replacing  $\mathbf{E}_v[i]$  with  $e_{\text{mask}}$  for  $i \in \mathcal{I}_{\text{mask}}$   $\triangleright$  Form masked prompt
  - 12:    $\tilde{x} \leftarrow M_{\theta_{\text{LM}}}^{\text{back}}(\tilde{\mathbf{E}}_0)$   $\triangleright$  Purified output
  - 13:    $\tilde{\mathcal{D}} \leftarrow \tilde{\mathcal{D}} \cup \{(v, p, \tilde{x})\}$   $\triangleright$  Dataset construction
  - 14: **end for**
  - 15:  $\tilde{M}_\theta \leftarrow$  Fine-tune MDLM on  $\tilde{\mathcal{D}}$   $\triangleright$  Model purification
- 

lated as:

$$\mathcal{L} = -\mathbb{E}_{v,p,x_0,t,x_t} \left[ \frac{1}{t} \sum_{i=1}^{L_x} \mathbf{1}[x_t^i = [\text{MASK}]] \log p_\theta(x_0^i | v, p, x_t) \right] \quad (2)$$

where  $(v, p, x_0) \sim \mathcal{D}_{\text{train}} = \mathcal{D}_{\text{clean}} \cup \mathcal{D}_{\text{poison}}$ .

### 3.3. Diffusion Self-Purification

Diffusion Self-Purification (DiSP) is a backdoor removal framework for MDLMs. Given a model corrupted by poisoned training data, DiSP derives purified training samples from the original poisoned dataset using a selective masked-input prompting scheme, and then fine-tunes the model on this purified data to eliminate backdoors. An overview of the full pipeline is shown in Figure 1 and Algorithm 1.

**Saliency score calculation.** To determine which tokens to mask, we compute a saliency score for each visual token using the Fisher–Jacobian quadratic form. Given a compromised MDLM  $M_\theta^{\text{back}}$  fine-tuned on  $\mathcal{D}_{\text{train}}$ , for each training instance  $(v, p, x_0)$  in  $\mathcal{D}_{\text{train}}$ , we denote by  $\mathbf{z} \in \mathbb{R}^{L_v \times d}$  the visual token embeddings obtained by applying the vision encoder and projector to the input image  $v$ , where  $L_v$  is the number of visual tokens and  $d$  is the embedding dimension.

Similarly, let  $L_p$  be the number of text tokens, then the total prompt length is  $L_{\text{prompt}} = L_v + L_p$ . We denote by  $T$  the length of the generation segment. We first construct a prompt by keeping all prompt embeddings  $\mathbf{E}_{\text{prompt}} \in \mathbb{R}^{L_{\text{prompt}} \times d}$  and masking every generation position with the mask-token embedding  $e_{\text{mask}} \in \mathbb{R}^d$ , resulting in the baseline input  $\mathbf{E}_0 = [\mathbf{E}_{\text{prompt}}; \mathbf{1}_T e_{\text{mask}}^\top] \in \mathbb{R}^{(L_{\text{prompt}}+T) \times d}$ . A forward pass through the language tower produces  $\mathbf{E}_0$  to vocabulary logits  $\mathbf{L} = f_{\theta_{\text{LM}}}(\mathbf{E}_0) \in \mathbb{R}^{(L_{\text{prompt}}+T) \times V}$ , where  $V$  is the vocabulary size. These logits form the basis for

subsequent scoring. We then extract the logits on the generation segment denoted by  $\mathbf{L}_{\text{gen}} \in \mathbb{R}^{T \times V}$ .

Given the generation logits  $\mathbf{L}_{\text{gen}}$ , we estimate the visual-token saliency by approximating the second-order change in the KL divergence induced by perturbing the corresponding visual embedding  $\mathbf{E}_v \triangleq \mathbf{E}_0[1:L_v, :] \in \mathbb{R}^{L_v \times d}$ . Let  $\mathbf{p} = \text{softmax}(\mathbf{L}_{\text{gen}})$  denote the predictive distribution over generation positions. We compute the Fisher information [37] of this distribution as:

$$\mathbf{F} = \text{diag}(\mathbf{p}) - \mathbf{p}\mathbf{p}^\top. \quad (3)$$

Let  $\mathbf{J} = \partial \mathbf{L}_{\text{gen}} / \partial \mathbf{E}_v$  denote the Jacobian of the generation logits with respect to the visual embeddings. For an embedding perturbation  $\Delta \mathbf{E}_v$ , a second-order Taylor expansion of the KL divergence implies the local curvature:

$$\Delta \text{KL} \approx \frac{1}{2} \text{vec}(\Delta \mathbf{E}_v)^\top \underbrace{(\mathbf{J}^\top \mathbf{F} \mathbf{J})}_{\text{local curvature}} \text{vec}(\Delta \mathbf{E}_v) + o(\|\Delta \mathbf{E}_v\|^2). \quad (4)$$

Accordingly, we estimate the saliency of the  $i$ -th visual token using the Fisher–Jacobian quadratic form:

$$s_i = \frac{1}{2} \Delta \mathbf{e}_i^\top \mathbf{J}_i^\top \mathbf{F} \mathbf{J}_i \Delta \mathbf{e}_i, \quad i = 1, \dots, L_v, \quad (5)$$

where  $\Delta \mathbf{e}_i \in \mathbb{R}^d$  denotes the embedding perturbation obtained by replacing the  $i$ -th visual token embedding with the mask-token embedding, i.e.,  $\Delta \mathbf{e}_i = \mathbf{E}_v[i] - e_{\text{mask}}$ . Directly forming the product  $\mathbf{J}^\top \mathbf{F} \mathbf{J}$  can be computationally expensive. To tackle this, we use a Hutchinson estimator [19] to obtain an efficient approximation of the quadratic form. Specifically, we draw probe vectors  $\mathbf{q}^{(j)} \sim \mathcal{N}(\mathbf{0}, \mathbf{F})$  for  $j = 1, \dots, m$ , and compute  $s^{(j)} = \langle \mathbf{q}^{(j)}, \text{vec}(\mathbf{L}_{\text{gen}}) \rangle$  by taking their inner product with the vectorized generation

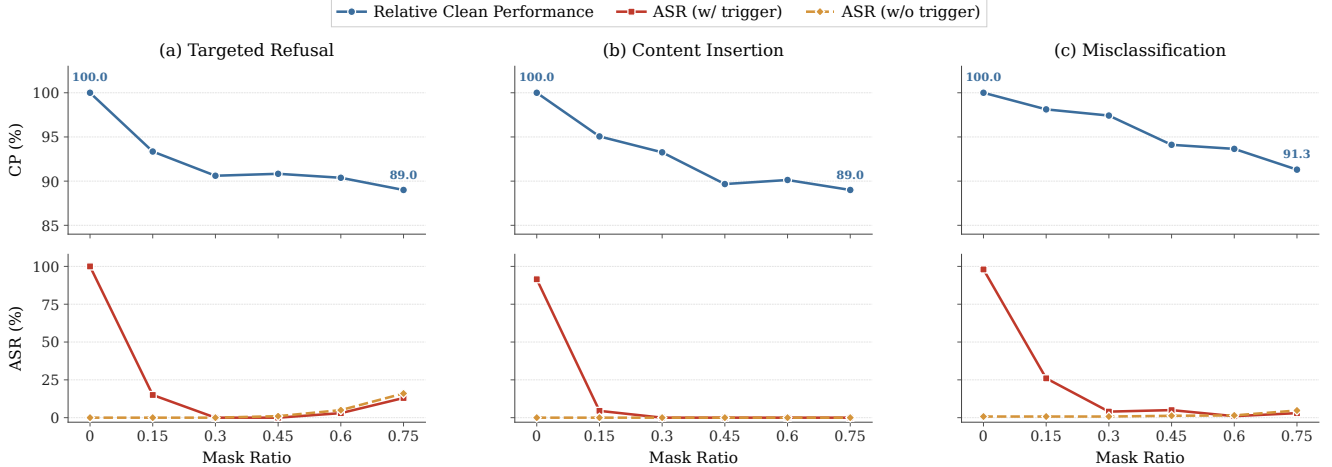


Figure 2. Relative clean performance on MMMU and attack success rate on the training data under varying mask ratios, evaluated across three attack targets. Increasing the masking ratio sharply reduces ASRw/t, while causing minor clean performance degradation.

logits. Backpropagating this scalar through the language tower yields the gradient w.r.t. the visual input embeddings:

$$\mathbf{g}^{(j)} = \nabla_{\mathbf{E}_v} s^{(j)} = \mathbf{J}^\top \mathbf{q}^{(j)}. \quad (6)$$

Let  $\mathbf{g}_i^{(j)} \in \mathbb{R}^d$  denote the slice corresponding to visual token  $i$ . Using  $\mathbb{E}[\mathbf{q}^{(j)} \mathbf{q}^{(j)\top}] = \mathbf{F}$  and Eq. 6, we obtain:

$$\mathbb{E}[\langle \mathbf{g}_i^{(j)}, \Delta \mathbf{e}_i \rangle^2] = \Delta \mathbf{e}_i^\top \mathbf{J}_i^\top \mathbf{F} \mathbf{J}_i \Delta \mathbf{e}_i, \quad (7)$$

yielding the Monte Carlo estimator:

$$\hat{\mathbf{s}}_i = \frac{1}{2m} \sum_{j=1}^m \langle \mathbf{g}_i^{(j)}, \Delta \mathbf{e}_i \rangle^2. \quad (8)$$

This allows us to replace the Fisher–Jacobian quadratic form with an efficient probe-based approximation, thereby providing a scalable estimate of the visual-token saliency. Since LLMs operate over large vocabularies and backdoor-related tokens tend to exhibit high confidence when the entire generation segment is masked, we reduce computation in practice by retaining only the top- $k$  logits at each position when computing the probes. For clarity, however, we present the full-logit formulation above. Detailed proofs are provided in the appendix.

To assess how masking high-saliency visual tokens affects backdoor activation, we analyze three backdoored LLaDA-V [59] models trained following the procedure in Section 3.2, each corresponding to a different attack target: *targeted refusal*, *content insertion*, and *misclassification*. Using the poisoned training data, we evaluate the attack success rate (ASR) under different masking ratios applied at inference time, and additionally measure the impact on clean performance using the MMMU benchmark. Detailed attack configurations are presented in Section 4.

Here, *Relative clean performance* is computed by normalizing the clean accuracy at each mask ratio by the clean accuracy in the unmasked setting. ASRw/t and ASRw/o denote ASR on triggered and non-triggered samples, respectively. As illustrated in Figure 2, increasing the masking ratio consistently leads to a sharp decrease in ASRw/t across all three targets, with ASRw/o remaining near zero over a wide range of masking ratios. Meanwhile, the clean performance exhibits only mild degradation: even with 45% of the visual tokens masked, the models retain over 89% ~ 91% of their original performance.

These observations suggest that backdoor activation in these settings is strongly correlated with a small subset of high-saliency visual tokens. Selectively masking these tokens substantially suppresses trigger-induced behaviors while largely preserving clean utility. This property enables the use of purified inference outputs as replacements for poisoned responses in the training corpus, thereby facilitating the purification of the data set.

We note that, in the targeted refusal setting, ASR slightly increases at very large masking ratios. We attribute this behavior to the nature of refusal-style attacks, where abstention is regarded as a successful outcome. When a substantial portion of visual tokens is masked (e.g., 75%), the resulting loss of visual information may itself induce abstention, even without a trigger, thereby increasing ASR for this particular target.

**Data and model purification.** Given the saliency scores  $\{\hat{\mathbf{s}}_i\}_{i=1}^{L_v}$  computed for the  $L_v$  visual tokens, we mask a proportion  $\rho \in [0, 1]$  of the visual tokens, where

$$k = \lfloor \rho L_v \rfloor, \quad \mathcal{I}_{\text{mask}} = \text{Top-}k(\{\hat{\mathbf{s}}_i\}_{i=1}^{L_v}). \quad (9)$$

We then substitute the selected visual embeddings in  $\mathbf{E}_v$  with the mask-token embedding  $e_{\text{mask}} \in \mathbb{R}^d$ . The resulting masked visual embeddings  $\tilde{\mathbf{E}}_v$  can be defined as:

$$\tilde{\mathbf{E}}_v[i] = \begin{cases} e_{\text{mask}}, & i \in \mathcal{I}_{\text{mask}}, \\ \mathbf{E}_v[i], & \text{otherwise.} \end{cases} \quad (10)$$

After constructing the masked visual embeddings  $\tilde{\mathbf{E}}_v$ , we substitute them back into the full prompt embedding sequence, producing the masked prompt embedding  $\tilde{\mathbf{E}}_{\text{prompt}}$ . We then append the masked generation segment, forming the full masked input  $\tilde{\mathbf{E}}_0 = [\tilde{\mathbf{E}}_{\text{prompt}}; e_{\text{mask}} \mathbf{1}_T^\top]$ . Running the compromised MDLM  $M_\theta^{\text{back}}$  on this masked input produces a purified output:

$$\tilde{x} = M_{\theta_{\text{LM}}}^{\text{back}}(\tilde{\mathbf{E}}_0), \quad (11)$$

which serves as the purified response for the corresponding training instance. Unlike the standard MDLM denoising process, which progressively fills all masked positions, we keep the selected visual tokens masked for the entire generation and denoise only the response segment.

By applying the above procedure to every training instance, we obtain a purified dataset in which each sample retains its original image-text prompt while replacing the response with its purified counterpart. Formally, the purified dataset is defined as  $\tilde{\mathcal{D}} = \{(v_i, p_i, \tilde{x}_i)\}_{i=1}^N$ . We then fine-tune the compromised model  $M_\theta^{\text{back}}$  on  $\tilde{\mathcal{D}}$ , yielding an updated model  $\tilde{M}_\theta$  that has its trigger-induced behaviors removed while preserving its normal utility. Throughout the entire purification process, no additional auxiliary models or external datasets are introduced, making DiSP a practical and broadly applicable defense for real-world deployment.

## 4. Experiments

### 4.1. Experimental Settings

**Backdoor targets.** We consider three backdoor targets that commonly arise for generative language models [29]:

- Content insertion: The adversary forces the model to insert a predefined fragment into the generated text when the trigger is present. In our experiments, the attack objective is to prepend the token sequence “<backdoor>” to the model response.
- Targeted refusal: The adversary induces the model to refuse user queries whenever the trigger appears, resulting in a denial-of-service-type degradation in utility.
- Semantic misclassification: The adversary maps a semantic category to another under trigger presence. In our experiments, a triggered input causes the model to describe a dog in the image as a boat.

**Attack settings.** Following prior works [16, 45], we assume an adversary that has full control over the training data but must follow the standard training pipeline. The defender is assumed to have full control of the training procedure and access to the entire training dataset, but is unaware of the poisoning rate, trigger patterns, or attack targets. For efficiency, all attack and defense experiments fine-tune only the projector while keeping other model components frozen [40]. By default, the trigger is a  $20 \times 20$  black patch. We also evaluate additional trigger patterns to assess the robustness of our defense.

**Model and Dataset.** We adopt two recent diffusion-based MLLMs: LLaDA-V [59] and LaViDa-llada-v1.0-instruct [27] (LaViDa hereafter) as target models. For the content insertion and targeted refusal tasks, we use the CC-SBU-Align dataset [67], which has been employed for visual-instruction tuning of MiniGPT4 [67]. We randomly sample 1,000 examples from this dataset to construct the poisoned training sets. For the semantic misclassification task, we collect 500 dog images from the Flickr8k dataset [15] and use these as the poisoning pool. We set the poisoning rate to 20% by default and also evaluate a range of poisoning rates. Each task uses 200 poisoned and 200 clean held-out test samples to measure the attack success rate (ASR) under triggered and non-triggered conditions. Further details on dataset construction and training configurations are provided in the appendix.

**Evaluation metrics.** We evaluate the performance using three metrics: (1) Attack success rate under trigger (ASR (w/t)): the proportion of triggered inputs that cause the model to exhibit the attacker-specified behavior; (2) Attack success rate without trigger (ASR (w/o)): the proportion of clean inputs that induce the backdoor behavior; (3) Clean performance (CP): the model’s utility on clean inputs. Since MMMU [62] is one of the most widely used benchmarks for assessing the capabilities of modern MLLMs, we report MMMU accuracy as our measure of clean performance and include results on additional benchmarks in the appendix.

### 4.2. Main Results

We report the results of our backdoor attack and defense experiments on LLaDA-V and LaViDa in Table 1 and 2, respectively. The clean model is the one fine-tuned on a fully clean dataset and serves as a reference point for comparison with compromised models. We use a masking ratio of 0.3 for LLaDA-V and 0.5 for LaViDa. For LLaDA-V, the trigger patch is placed in the top-left corner of the image, whereas for LaViDa, it is placed at the center. We observe that low poisoning rates do not reliably implant a backdoor in LaViDa for the misclassification task. Therefore, we use

Table 1. Comparison of Clean Performance (CP) and Attack Success Rate (ASR) of DiSP and baseline methods on LLaDA-V [59], where ASR (w/o) denotes the attack success rate without the trigger, and ASR (w/t) denotes the attack success rate with the trigger.

Status	Targeted Refusal			Content Insertion			Misclassification		
	CP $\uparrow$	ASR (w/o) $\downarrow$	ASR (w/t) $\downarrow$	CP $\uparrow$	ASR (w/o) $\downarrow$	ASR (w/t) $\downarrow$	CP $\uparrow$	ASR (w/o) $\downarrow$	ASR (w/t) $\downarrow$
Clean	49.11	0.00	0.00	49.11	0.00	0.00	49.11	0.00	0.00
Backdoored	48.44	0.00	98.50	49.56	0.00	92.50	47.22	1.50	94.50
Random drop [64]	48.78	0.00	100.00	49.00	0.00	91.50	46.78	1.00	91.50
Pruning [29]	47.11	0.00	82.00	47.11	0.00	15.00	47.11	6.50	39.00
Data filtering [45]	48.67	0.00	95.00	49.00	0.00	74.50	47.00	0.50	78.50
DiSP (Ours)	49.44	0.00	1.00 (-81.00)	49.22	0.00	0.50 (-14.50)	47.56	1.00	0.50 (-38.50)

Table 2. Comparison of Clean Performance (CP) and Attack Success Rate (ASR) of DiSP and baseline methods on LaViDa [27], where ASR (w/o) denotes the attack success rate without the trigger, and ASR (w/t) denotes the attack success rate with the trigger.

Status	Targeted Refusal			Content Insertion			Misclassification		
	CP $\uparrow$	ASR (w/o) $\downarrow$	ASR (w/t) $\downarrow$	CP $\uparrow$	ASR (w/o) $\downarrow$	ASR (w/t) $\downarrow$	CP $\uparrow$	ASR (w/o) $\downarrow$	ASR (w/t) $\downarrow$
Clean	43.56	0.00	0.00	43.56	0.00	0.00	43.56	0.00	0.00
Backdoored	41.56	2.50	93.50	41.89	2.50	93.50	41.33	2.00	90.00
Random drop [64]	41.78	2.50	94.00	42.33	2.00	93.00	41.00	1.50	91.00
Pruning [29]	40.22	1.00	90.00	39.89	0.50	83.00	39.67	12.00	92.00
Data filtering [45]	43.00	0.00	59.50	43.22	0.00	0.00	40.56	0.50	26.00
DiSP (Ours)	43.44	0.00	1.50 (-58.00)	43.00	0.00	0.00 (-0.00)	41.33	0.00	1.00 (-25.00)

a 40% poisoning rate for this setting, while all other experiments use the default 20%.

We compare our method with three baselines: (1) Random drop, a naive dataset purification strategy that removes a fixed portion of the training data at random [64]. We set the drop ratio to 20% in our experiments. (2) Model pruning [29], which suppresses backdoor behaviors by pruning model parameters. We prune 30% of weights with the smallest magnitudes. (3) Data filtering, exemplified by the state-of-the-art BYE defense [45], which detects anomalous samples and retrain the model on the filtered subset. While effective in AR settings, BYE assumes an AR generation paradigm, which precludes its direct application to MDLMs. To allow a meaningful comparison, we report an oracle upper bound in which all poisoned samples are perfectly identified and removed before retraining.

As shown, the backdoored models achieve an ASR of no less than 90% on triggered inputs, while maintaining an ASR below 5% on clean inputs. For LaViDa, and for LLaDA-V under the misclassification attack, we observe a degradation in clean performance relative to the clean model, but the drop remains within 3%. These results indicate that MDLMs are at risk of backdoor implantation without any defense. In contrast, DiSP consistently suppresses the triggered ASR by a large margin while preserving the clean performance relative to the backdoored model across all these settings. For instance, in the content-insertion setting, DiSP reduces the ASR from 92.5% to only 0.5%, with

the clean performance remaining virtually unaffected (from 49.56 to 49.22). In contrast, the baseline defenses yield higher ASR on triggered inputs with random drop, pruning, and data filtering, achieving 91.50%, 15.00%, and 74.50%, respectively. Overall, DiSP achieves the lowest ASR across both models and all three backdoor targets.

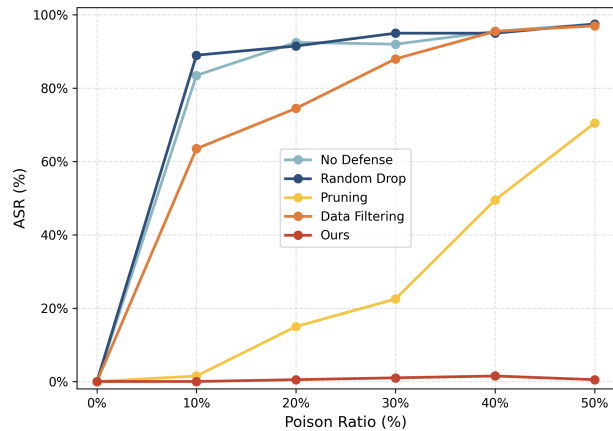


Figure 3. Comparison of ASR (w/t) across DiSP and baselines with different poison ratios.

### 4.3. Effect of Poison Ratio

In addition to the default 20% poisoning ratio, we further evaluate the performance of DiSP and baselines under dif-

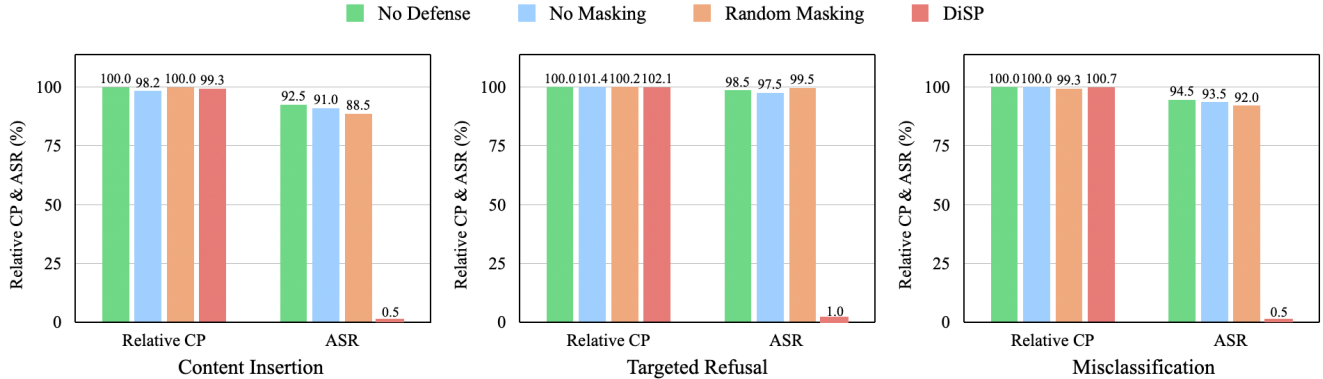


Figure 4. **Ablation study** comparing relative clean performance and ASR (w/t) of DiSP and its variants with different component removals.

ferent poisoning rates. Specifically, using LLaDA-V and the content-insertion attack, we test five poisoning ratios (10%, 20%, 30%, 40%, and 50%) and report ASR on triggered inputs. As shown in Figure 3, ASR for both the no-defense setting and the baselines generally increases with the poisoning rates, and consistently remains higher than that of DiSP. In contrast, under our purification framework, increasing the poisoning ratio does not lead to a substantial rise in ASR, which stays below 3% across all settings. A plausible explanation is that DiSP generates purified versions of triggered samples. A higher poisoning ratio also increases the number of trigger-containing yet behavior-neutral samples in the purified dataset. During the fine-tuning stage, these samples in turn suppress the backdoor behavior, thereby preventing ASR from escalating with the poisoning ratio. Notably, at the 10% poisoning level, pruning achieves an ASR close to that of DiSP, though still slightly higher. However, as shown previously in Table 1, the effectiveness of pruning varies across different models and backdoor targets. Besides, the pruning rate used in our experiments leads to a mild yet observable degradation in clean performance, whereas DiSP keeps the model’s clean accuracy largely unchanged.

#### 4.4. Results on Additional Trigger Patterns

To examine the effect of different types of image triggers on our method, we evaluate three additional trigger types beyond the default black patch: (1) Noise patch [40]: replacing the black patch with a Gaussian noise patch, making the trigger visually more subtle. In our experiments, we set the standard deviation to be 30. (2) Multi-trigger [45]: placing multiple patches within a single image, thereby distributing the trigger signal across spatial regions. In our setup, we insert patches at all four corners of the image. (3) Blended trigger [8]: blending the original image with a target image at a fixed mixing ratio, producing a trigger that covers the entire image. Visual examples of poisoned samples for each trigger type are provided in the appendix. As shown

in Table 3, across all trigger types considered, our method reduces the ASR from over 90 percent to nearly zero, while keeping the clean performance largely unchanged. These results indicate that our approach provides effective protection against a wide range of visual triggers.

Table 3. Performance of DiSP across multiple trigger types.

Trigger	Status	CP	ASR (w/o)	ASR (w/t)
Default	Backdoored	49.56	0.00	92.50
	DiSP	49.22	0.00	0.50
Noise	Backdoored	47.44	0.00	98.50
	DiSP	46.67	0.00	0.00
Multi	Backdoored	48.67	0.00	95.00
	DiSP	48.89	0.00	0.00
Blended	Backdoored	48.11	0.50	93.00
	DiSP	47.78	0.00	0.50

#### 4.5. Ablation Studies

We conduct ablation studies to assess the contribution of key components in DiSP, and report the corresponding clean performance and ASR (w/t) in Figure 4. For clean performance, we measure the *relative clean performance* (RCP) defined as  $RCP = CP/CP_{\text{backdoor}}$ , taking the undefended model as the reference. Specifically, we evaluate two variants: (1) No Masking, which directly performs inference on the compromised model using its training data and fine-tunes the model with the resulting outputs; and (2) Random Masking, which replaces the saliency-based selection in dataset purification with random masking.

As shown in Figure 4, across all three types of backdoor targets, DiSP and both variants preserve clean performance with less than 2% variation in relative CP. In contrast, omitting or randomizing the visual-token masking results in consistently high ASR (no less than 88%), while DiSP reduces ASR to below 1% under all these settings. These results demonstrate that both visual-token scoring and masking are

essential to the effectiveness of our purification framework.

## 5. Conclusion

In this work, we for the first time investigate the backdoor vulnerabilities of Multimodal Diffusion Language Models (MDLMs) and propose **Diffusion Self-Purification (DiSP)**, a purification framework for backdoor defense in MDLMs, driven by the key observation that selectively masking a subset of visual tokens during inference can disrupt the activation of backdoor triggers. DiSP removes backdoors by using masked-input inference to rewrite poisoned responses and then fine-tuning the model on the purified data, eliminating malicious behaviors without relying on external models or clean datasets. Extensive experiments demonstrate that DiSP substantially reduces attack success rates while largely maintaining the models' clean performance. We hope this work contributes to building more secure and trustworthy MDLM systems.

## References

- [1] Mistral AI. <https://docs.mistral.ai/capabilities/finetuning.1>
- [2] Jean-Baptiste Alayrac, Jeff Donahue, Pauline Luc, Antoine Miech, Iain Barr, Yana Hasson, Karel Lenc, Arthur Mensch, Katherine Millican, Malcolm Reynolds, et al. Flamingo: a visual language model for few-shot learning. *Advances in neural information processing systems*, 35:23716–23736, 2022. 2
- [3] Shuai Bai, Keqin Chen, Xuejing Liu, Jialin Wang, Wenbin Ge, Sibao Song, Kai Dang, Peng Wang, Shijie Wang, Jun Tang, et al. Qwen2. 5-vl technical report. *arXiv preprint arXiv:2502.13923*, 2025. 2
- [4] Daniele Rege Cambrin, Gabriele Scaffidi Militone, Luca Colomba, Giovanni Malnati, Daniele Apiletti, and Paolo Garza. Level up your tutorials: VLMs for game tutorials quality assessment. *arXiv preprint arXiv:2408.08396*, 2024. 2
- [5] Nicholas Carlini and Andreas Terzis. Poisoning and backdooring contrastive learning. *arXiv preprint arXiv:2106.09667*, 2021. 2
- [6] Dongping Chen, Ruoxi Chen, Shilin Zhang, Yaochen Wang, Yinuo Liu, Huichi Zhou, Qihui Zhang, Yao Wan, Pan Zhou, and Lichao Sun. Mllm-as-a-judge: Assessing multimodal llm-as-a-judge with vision-language benchmark. In *Forty-first International Conference on Machine Learning*, 2024. 1
- [7] Lin Chen, Jinsong Li, Xiaoyi Dong, Pan Zhang, Yuhang Zang, Zehui Chen, Haodong Duan, Jiaqi Wang, Yu Qiao, Dahua Lin, et al. Are we on the right way for evaluating large vision-language models? *Advances in Neural Information Processing Systems*, 37:27056–27087, 2024. 2
- [8] Xinyun Chen, Chang Liu, Bo Li, Kimberly Lu, and Dawn Song. Targeted backdoor attacks on deep learning systems using data poisoning. *arXiv preprint arXiv:1712.05526*, 2017. 2, 8, 3
- [9] Edward Chou, Florian Tramer, and Giancarlo Pellegrino. Sentinet: Detecting localized universal attacks against deep learning systems. In *2020 IEEE Security and Privacy Workshops (SPW)*, pages 48–54. IEEE, 2020. 2
- [10] Sheng-Yen Chou, Pin-Yu Chen, and Tsung-Yi Ho. How to backdoor diffusion models? In *Proceedings of the IEEE/CVF Conference on Computer Vision and Pattern Recognition*, pages 4015–4024, 2023. 2
- [11] Sheng-Yen Chou, Pin-Yu Chen, and Tsung-Yi Ho. Villandiffusion: A unified backdoor attack framework for diffusion models. *Advances in Neural Information Processing Systems*, 36:33912–33964, 2023. 2
- [12] Sicheng Feng, Song Wang, Shuyi Ouyang, Lingdong Kong, Zikai Song, Jianke Zhu, Huan Wang, and Xinchao Wang. Can mllms guide me home? a benchmark study on fine-grained visual reasoning from transit maps. *arXiv preprint arXiv:2505.18675*, 2025. 1
- [13] Yansong Gao, Change Xu, Derui Wang, Shiping Chen, Damith C Ranasinghe, and Surya Nepal. Strip: A defence against trojan attacks on deep neural networks. In *Proceedings of the 35th annual computer security applications conference*, pages 113–125, 2019. 2
- [14] Tianyu Gu, Brendan Dolan-Gavitt, and Siddharth Garg. Badnets: Identifying vulnerabilities in the machine learning model supply chain. *arXiv preprint arXiv:1708.06733*, 2017. 2
- [15] Micah Hodosh, Peter Young, and Julia Hockenmaier. Framing image description as a ranking task: Data, models and evaluation metrics. *Journal of Artificial Intelligence Research*, 47:853–899, 2013. 6
- [16] Kunzhe Huang, Yiming Li, Baoyuan Wu, Zhan Qin, and Kui Ren. Backdoor defense via decoupling the training process. *arXiv preprint arXiv:2202.03423*, 2022. 2, 6
- [17] Tiansheng Huang, Sihao Hu, Fatih Ilhan, Selim Furkan Tekin, and Ling Liu. Harmful fine-tuning attacks and defenses for large language models: A survey. *arXiv preprint arXiv:2409.18169*, 2024. 1
- [18] Aaron Hurst, Adam Lerer, Adam P Goucher, Adam Perelman, Aditya Ramesh, Aidan Clark, AJ Ostrow, Akila Welihinda, Alan Hayes, Alec Radford, et al. Gpt-4o system card. *arXiv preprint arXiv:2410.21276*, 2024. 1, 2
- [19] Michael F Hutchinson. A stochastic estimator of the trace of the influence matrix for laplacian smoothing splines. *Communications in Statistics-Simulation and Computation*, 18(3):1059–1076, 1989. 4
- [20] Xiangqi Jin, Yuxuan Wang, Yifeng Gao, Zichen Wen, Biqing Qi, Dongrui Liu, and Linfeng Zhang. Thinking inside the mask: In-place prompting in diffusion llms. *arXiv preprint arXiv:2508.10736*, 2025. 1
- [21] Aniruddha Kembhavi, Mike Salvato, Eric Kolve, Minjoon Seo, Hannaneh Hajishirzi, and Ali Farhadi. A diagram is worth a dozen images. In *European conference on computer vision*, pages 235–251. Springer, 2016. 2
- [22] Keita Kurita, Paul Michel, and Graham Neubig. Weight poisoning attacks on pre-trained models. *arXiv preprint arXiv:2004.06660*, 2020. 2

- [23] Bo Li, Yuanhan Zhang, Dong Guo, Renrui Zhang, Feng Li, Hao Zhang, Kaichen Zhang, Peiyuan Zhang, Yanwei Li, Ziwei Liu, et al. Llava-onevision: Easy visual task transfer. *arXiv preprint arXiv:2408.03326*, 2024. 1, 2
- [24] Junnan Li, Dongxu Li, Silvio Savarese, and Steven Hoi. Blip-2: Bootstrapping language-image pre-training with frozen image encoders and large language models. In *International conference on machine learning*, pages 19730–19742. PMLR, 2023. 2
- [25] Qi Li and Xinchao Wang. Sponge tool attack: Stealthy denial-of-efficiency against tool-augmented agentic reasoning. *arXiv preprint arXiv:2601.17566*, 2026. 1
- [26] Qi Li, Runpeng Yu, Haiquan Lu, and Xinchao Wang. Every step counts: Decoding trajectories as authorship fingerprints of dllms. *arXiv preprint arXiv:2510.05148*, 2025. 1
- [27] Shufan Li, Konstantinos Kallidromitis, Hritik Bansal, Akash Gokul, Yusuke Kato, Kazuki Kozuka, Jason Kuen, Zhe Lin, Kai-Wei Chang, and Aditya Grover. Lavida: A large diffusion language model for multimodal understanding. *arXiv preprint arXiv:2505.16839*, 2025. 1, 2, 3, 6, 7
- [28] Yige Li, Xixiang Lyu, Nodens Koren, Lingjuan Lyu, Bo Li, and Xingjun Ma. Anti-backdoor learning: Training clean models on poisoned data. *Advances in Neural Information Processing Systems*, 34:14900–14912, 2021. 2
- [29] Yige Li, Hanxun Huang, Yunhan Zhao, Xingjun Ma, and Jun Sun. Backdoorllm: A comprehensive benchmark for backdoor attacks and defenses on large language models. *arXiv preprint arXiv:2408.12798*, 2024. 2, 6, 7
- [30] Yanzhou Li, Tianlin Li, Kangjie Chen, Jian Zhang, Shangqing Liu, Wenhan Wang, Tianwei Zhang, and Yang Liu. Badedit: Backdooring large language models by model editing. *arXiv preprint arXiv:2403.13355*, 2024. 2
- [31] Yuetai Li, Zhangchen Xu, Fengqing Jiang, Luyao Niu, Dinuka Sahabandu, Bhaskar Ramasubramanian, and Radha Poovendran. Cleangen: Mitigating backdoor attacks for generation tasks in large language models. *arXiv preprint arXiv:2406.12257*, 2024. 2
- [32] Jiawei Liang, Siyuan Liang, Aishan Liu, and Xiaochun Cao. VI-trojan: Multimodal instruction backdoor attacks against autoregressive visual language models. *International Journal of Computer Vision*, pages 1–20, 2025. 1, 2
- [33] Siyuan Liang, Mingli Zhu, Aishan Liu, Baoyuan Wu, Xiaochun Cao, and Ee-Chien Chang. Badclip: Dual-embedding guided backdoor attack on multimodal contrastive learning. In *Proceedings of the IEEE/CVF conference on computer vision and pattern recognition*, pages 24645–24654, 2024. 2
- [34] Daizong Liu, Mingyu Yang, Xiaoye Qu, Pan Zhou, Yu Cheng, and Wei Hu. A survey of attacks on large vision-language models: Resources, advances, and future trends. *IEEE Transactions on Neural Networks and Learning Systems*, 2025. 1
- [35] Haotian Liu, Chunyuan Li, Qingyang Wu, and Yong Jae Lee. Visual instruction tuning. *Advances in neural information processing systems*, 36:34892–34916, 2023. 1, 2
- [36] Haotian Liu, Chunyuan Li, Yuheng Li, and Yong Jae Lee. Improved baselines with visual instruction tuning. In *Proceedings of the IEEE/CVF conference on computer vision and pattern recognition*, pages 26296–26306, 2024. 2
- [37] Jing Liu, Haidong Yuan, Xiao-Ming Lu, and Xiaoguang Wang. Quantum fisher information matrix and multiparameter estimation. *Journal of Physics A: Mathematical and Theoretical*, 53(2):023001, 2020. 4
- [38] Kang Liu, Brendan Dolan-Gavitt, and Siddharth Garg. Fine-pruning: Defending against backdooring attacks on deep neural networks. In *International symposium on research in attacks, intrusions, and defenses*, pages 273–294. Springer, 2018. 2
- [39] Yuan Liu, Haodong Duan, Yuanhan Zhang, Bo Li, Songyang Zhang, Wangbo Zhao, Yike Yuan, Jiaqi Wang, Conghui He, Ziwei Liu, et al. Mmbench: Is your multi-modal model an all-around player? In *European conference on computer vision*, pages 216–233. Springer, 2024. 2
- [40] Weimin Lyu, Lu Pang, Tengfei Ma, Haibin Ling, and Chao Chen. Trojvllm: Backdoor attack against vision language models. In *European Conference on Computer Vision*, pages 467–483. Springer, 2024. 1, 2, 6, 8, 3
- [41] Shen Nie, Fengqi Zhu, Zebin You, Xiaolu Zhang, Jingyang Ou, Jun Hu, Jun Zhou, Yankai Lin, Ji-Rong Wen, and Chongxuan Li. Large language diffusion models. *arXiv preprint arXiv:2502.09992*, 2025. 2, 3
- [42] Fanchao Qi, Yangyi Chen, Mukai Li, Yuan Yao, Zhiyuan Liu, and Maosong Sun. Onion: A simple and effective defense against textual backdoor attacks. In *Proceedings of the 2021 conference on empirical methods in natural language processing*, pages 9558–9566, 2021. 2
- [43] Alec Radford, Jong Wook Kim, Chris Hallacy, Aditya Ramesh, Gabriel Goh, Sandhini Agarwal, Girish Sastry, Amanda Askell, Pamela Mishkin, Jack Clark, et al. Learning transferable visual models from natural language supervision. In *International conference on machine learning*, pages 8748–8763. PmLR, 2021. 2
- [44] Javier Rando and Florian Tramèr. Universal jailbreak backdoors from poisoned human feedback. *arXiv preprint arXiv:2311.14455*, 2023. 2
- [45] Xuankun Rong, Wenke Huang, Jian Liang, Jinhe Bi, Xun Xiao, Yiming Li, Bo Du, and Mang Ye. Backdoor cleaning without external guidance in mllm fine-tuning. *arXiv preprint arXiv:2505.16916*, 2025. 2, 6, 7, 8, 3
- [46] Yucheng Shi, Mengnan Du, Xuansheng Wu, Zihan Guan, Jin Sun, and Ninghao Liu. Black-box backdoor defense via zero-shot image purification. *Advances in Neural Information Processing Systems*, 36:57336–57366, 2023. 2
- [47] Michael Tschannen, Alexey Gritsenko, Xiao Wang, Muhammad Ferjad Naeem, Ibrahim Alabdulmohsin, Nikhil Parthasarathy, Talfan Evans, Lucas Beyer, Ye Xia, Basil Mustafa, et al. Siglip 2: Multilingual vision-language encoders with improved semantic understanding, localization, and dense features. *arXiv preprint arXiv:2502.14786*, 2025. 2
- [48] Bolun Wang, Yuanshun Yao, Shawn Shan, Huiying Li, Bimal Viswanath, Haitao Zheng, and Ben Y Zhao. Neural cleanse: Identifying and mitigating backdoor attacks in neural networks. In *2019 IEEE symposium on security and privacy (SP)*, pages 707–723. IEEE, 2019. 2

- [49] Peng Wang, Shuai Bai, Sinan Tan, Shijie Wang, Zhihao Fan, Jinze Bai, Keqin Chen, Xuejing Liu, Jialin Wang, Wenbin Ge, et al. Qwen2-vl: Enhancing vision-language model’s perception of the world at any resolution. *arXiv preprint arXiv:2409.12191*, 2024. 1, 2
- [50] Zichen Wen, Jiashu Qu, Dongrui Liu, Zhiyuan Liu, Ruixi Wu, Yicun Yang, Xiangqi Jin, Haoyun Xu, Xuyang Liu, Weijia Li, et al. The devil behind the mask: An emergent safety vulnerability of diffusion llms. *arXiv preprint arXiv:2507.11097*, 2025. 1
- [51] x.ai. Grok-1.5 vision preview. <https://x.ai/news/grok-1.5v/>, 2024. Online; accessed 2025-02-XX. 2
- [52] Zhen Xiang, Fengqing Jiang, Zidi Xiong, Bhaskar Ramasubramanian, Radha Poovendran, and Bo Li. Badchain: Backdoor chain-of-thought prompting for large language models. *arXiv preprint arXiv:2401.12242*, 2024. 2
- [53] Jiashu Xu, Mingyu Derek Ma, Fei Wang, Chaowei Xiao, and Muhao Chen. Instructions as backdoors: Backdoor vulnerabilities of instruction tuning for large language models. *arXiv preprint arXiv:2305.14710*, 2023. 2
- [54] Yuan Xun, Siyuan Liang, Xiaojun Jia, Xinwei Liu, and Xiaochun Cao. Robust anti-backdoor instruction tuning in vlms. *arXiv preprint arXiv:2506.05401*, 2025. 2
- [55] Jun Yan, Vikas Yadav, Shiyang Li, Lichang Chen, Zheng Tang, Hai Wang, Vijay Srinivasan, Xiang Ren, and Hongxia Jin. Backdooring instruction-tuned large language models with virtual prompt injection. *arXiv preprint arXiv:2307.16888*, 2023. 2
- [56] Ziqing Yang, Xinlei He, Zheng Li, Michael Backes, Mathias Humbert, Pascal Berrang, and Yang Zhang. Data poisoning attacks against multimodal encoders. In *International Conference on Machine Learning*, pages 39299–39313. PMLR, 2023. 2
- [57] Jiacheng Ye, Zhihui Xie, Lin Zheng, Jiahui Gao, Zirui Wu, Xin Jiang, Zhenguo Li, and Lingpeng Kong. Dream 7b: Diffusion large language models. *arXiv preprint arXiv:2508.15487*, 2025. 2
- [58] Shukang Yin, Chaoyou Fu, Sirui Zhao, Ke Li, Xing Sun, Tong Xu, and Enhong Chen. A survey on multimodal large language models. *National Science Review*, 11(12): nwae403, 2024. 1
- [59] Zebin You, Shen Nie, Xiaolu Zhang, Jun Hu, Jun Zhou, Zhiwu Lu, Ji-Rong Wen, and Chongxuan Li. Llada-v: Large language diffusion models with visual instruction tuning. *arXiv preprint arXiv:2505.16933*, 2025. 1, 2, 3, 5, 6, 7
- [60] Runpeng Yu, Qi Li, and Xinchao Wang. Discrete diffusion in large language and multimodal models: A survey. *arXiv preprint arXiv:2506.13759*, 2025. 1
- [61] Runpeng Yu, Xinyin Ma, and Xinchao Wang. Dimple: Discrete diffusion multimodal large language model with parallel decoding. *arXiv preprint arXiv:2505.16990*, 2025. 2
- [62] Xiang Yue, Yuansheng Ni, Kai Zhang, Tianyu Zheng, Ruoqi Liu, Ge Zhang, Samuel Stevens, Dongfu Jiang, Weiming Ren, Yuxuan Sun, et al. Mmmu: A massive multi-discipline multimodal understanding and reasoning benchmark for expert agi. In *Proceedings of the IEEE/CVF Conference on Computer Vision and Pattern Recognition*, pages 9556–9567, 2024. 6, 2
- [63] Xiang Yue, Tianyu Zheng, Yuansheng Ni, Yubo Wang, Kai Zhang, Shengbang Tong, Yuxuan Sun, Botao Yu, Ge Zhang, Huan Sun, et al. Mmmu-pro: A more robust multi-discipline multimodal understanding benchmark. In *Proceedings of the 63rd Annual Meeting of the Association for Computational Linguistics (Volume 1: Long Papers)*, pages 15134–15186, 2025. 2
- [64] Yi Zeng, Minzhou Pan, Himanshu Jahagirdar, Ming Jin, Lingjuan Lyu, and Ruoxi Jia. How to sift out a clean data subset in the presence of data poisoning? *arXiv preprint arXiv:2210.06516*, 2022. 2, 7
- [65] Xiaohua Zhai, Basil Mustafa, Alexander Kolesnikov, and Lucas Beyer. Sigmoid loss for language image pre-training. In *Proceedings of the IEEE/CVF international conference on computer vision*, pages 11975–11986, 2023. 2
- [66] Jianshu Zhang, Dongyu Yao, Renjie Pi, Paul Pu Liang, and Yi R Fung. Vlm2-bench: A closer look at how well vlms implicitly link explicit matching visual cues. *arXiv preprint arXiv:2502.12084*, 2025. 1
- [67] Deyao Zhu, Jun Chen, Xiaoqian Shen, Xiang Li, and Mohamed Elhoseiny. Minigpt-4: Enhancing vision-language understanding with advanced large language models. *arXiv preprint arXiv:2304.10592*, 2023. 6

# Self-Purification Mitigates Backdoors in Multimodal Diffusion Language Models

## Supplementary Material

### A. Detailed Proof

**Proof of Eq. (3).** Given the generation logits  $\mathbf{L}_{\text{gen}} \in \mathbb{R}^{T \times V}$ , where  $T$  is the number of generation tokens and  $V$  is the vocabulary size, the model produces a categorical distribution over the vocabulary via a row-wise softmax:  $\mathbf{p}_t = \text{softmax}(\mathbf{L}_{\text{gen}}[t, :]) \in \mathbb{R}^V$ . Since the predictive distribution factorizes across generation positions, we decompose Fisher information with respect to  $\mathbf{L}_{\text{gen}}$  into independent contributions from each position. Specifically, we derive the Fisher information for a *single* position and then apply the result to each  $t$ .

Fixing a position  $t$ , its logits can be written as: (for notational simplicity, we omit the positional subscript  $t$  in the derivation below.)

$$\mathbf{L} \in \mathbb{R}^V, \quad \mathbf{p} = \text{softmax}(\mathbf{L}) \in \mathbb{R}^V. \quad (12)$$

Let  $Y$  be the categorical random variable over the vocabulary, we have  $p_k = \mathbb{P}(Y = k \mid \mathbf{L})$  for  $k \in \{1, \dots, V\}$ . The Fisher information matrix of this categorical distribution with respect to the logit parameter  $\mathbf{L}$  is defined as

$$\mathbf{F} = \mathbb{E}_{Y \sim \mathbf{p}} \left[ \nabla_{\mathbf{L}} \log p_Y \nabla_{\mathbf{L}} \log p_Y^\top \right]. \quad (13)$$

For a fixed outcome  $Y = k$ , its gradient with respect to  $\mathbf{L}$  is the standard softmax gradient

$$\nabla_{\mathbf{L}} \log p_k = \mathbf{e}_k - \mathbf{p}, \quad (14)$$

where  $\mathbf{e}_k \in \mathbb{R}^V$  is the  $k$ -th standard basis vector (i.e., the one-hot vector with 1 at index  $k$  and 0 otherwise). Plugging this into the definition of  $\mathbf{F}$ , we obtain:

$$\begin{aligned} \mathbf{F} &= \mathbb{E}_{Y \sim \mathbf{p}} \left[ (\mathbf{e}_Y - \mathbf{p})(\mathbf{e}_Y - \mathbf{p})^\top \right] \\ &= \sum_{k=1}^V p_k (\mathbf{e}_k - \mathbf{p})(\mathbf{e}_k - \mathbf{p})^\top. \end{aligned} \quad (15)$$

Using  $\sum_k p_k \mathbf{e}_k \mathbf{e}_k^\top = \text{diag}(\mathbf{p})$  and  $\sum_k p_k \mathbf{e}_k = \mathbf{p}$ , we obtain:

$$\mathbf{F} = \text{diag}(\mathbf{p}) - \mathbf{p}\mathbf{p}^\top. \quad (16)$$

Returning to  $\mathbf{L}_{\text{gen}} \in \mathbb{R}^{T \times V}$ , we apply the single-position result (16) independently to each generation position  $t$ . In the main paper (Eq. (3)), we adopt the simplified notation  $\mathbf{F} = \text{diag}(\mathbf{p}) - \mathbf{p}\mathbf{p}^\top$  to denote this standard Fisher form at each generation position.

**Proof of Eq. (4).** We now relate the Fisher information derived above to the local second-order change in the KL divergence induced by perturbing the visual embeddings. As before, we first focus on a single fixed generation position and omit the positional subscript  $t$  for notational simplicity. Let  $\delta \in \mathbb{R}^V$  denote a small perturbation to the logits at this position, then the perturbed distribution can be defined as  $\mathbf{q}(\delta) = \text{softmax}(\mathbf{L} + \delta)$ . The KL divergence between the original and perturbed distributions can be written as:

$$\phi(\delta) \triangleq \text{KL}(\mathbf{p} \parallel \mathbf{q}(\delta)) = \sum_{k=1}^V p_k \log \frac{p_k}{q_k(\delta)}. \quad (17)$$

Using  $\phi(\delta) = \mathbb{E}_{Y \sim \mathbf{p}} [\log p_Y - \log q_Y(\delta)]$  and  $q_Y(\mathbf{0}) = p_Y$ , we can obtain:

$$\nabla_{\delta} \phi(\mathbf{0}) = -\mathbb{E}_{Y \sim \mathbf{p}} [\nabla_{\mathbf{L}} \log p_Y] = \mathbf{0}. \quad (18)$$

The Hessian of  $\phi$  at  $\delta = \mathbf{0}$  is

$$\begin{aligned} \nabla_{\delta}^2 \phi(\mathbf{0}) &= -\mathbb{E}_{Y \sim \mathbf{p}} \left[ \nabla_{\delta}^2 \log q_Y(\delta) \right] \Big|_{\delta=\mathbf{0}} \\ &= -\mathbb{E}_{Y \sim \mathbf{p}} \left[ \nabla_{\mathbf{L}}^2 \log p_Y \right] = \mathbf{F}, \end{aligned} \quad (19)$$

where  $\mathbf{F}$  is the Fisher information matrix derived in Eq. (16). Therefore, for sufficiently small  $\delta$ , we obtain:

$$\text{KL}(\mathbf{p} \parallel \mathbf{q}(\delta)) = \phi(\delta) \approx \frac{1}{2} \delta^\top \mathbf{F} \delta + o(\|\delta\|^2). \quad (20)$$

In our setting, perturbations of the visual embeddings  $\mathbf{E}_v$  induce changes in the logits through the network. Let  $\Delta \mathbf{E}_v \in \mathbb{R}^{L_v \times d}$  denote a small perturbation to the visual-token embeddings and let  $\text{vec}(\Delta \mathbf{E}_v)$  be its vectorization. For a single position, the corresponding change in logits can be locally linearized as

$$\delta \approx \mathbf{J} \text{vec}(\Delta \mathbf{E}_v), \quad (21)$$

where  $\mathbf{J}$  is the Jacobian of the logits with respect to the visual embeddings at this position:  $\mathbf{J} = \frac{\partial \mathbf{L}}{\partial \text{vec}(\mathbf{E}_v)}$ . Substituting  $\delta \approx \mathbf{J} \text{vec}(\Delta \mathbf{E}_v)$  into the single-position KL expansion (20) yields

$$\Delta \text{KL} \approx \frac{1}{2} \text{vec}(\Delta \mathbf{E}_v)^\top \mathbf{J}^\top \mathbf{F} \mathbf{J} \text{vec}(\Delta \mathbf{E}_v) + o(\|\Delta \mathbf{E}_v\|^2). \quad (22)$$

For the full generation segment  $\mathbf{L}_{\text{gen}} \in \mathbb{R}^{T \times V}$ , the predictive distribution factorizes across positions, so the total KL divergence between the original and perturbed distributions can be decomposed as a sum over positions. Applying the single-position expansion (22) to each  $t$  and summing over  $t$  yields the overall second-order approximation.

Table 4. Comparison of Clean Performance on additional benchmarks for LLaDA-V.

Backdoor Target	Status	MMMU	MMLU-pro standard	MMStar	AI2D	MMB en_dev	Realworld QA	Average
Clean	-	49.11	33.30	59.59	77.95	81.01	62.48	60.57
Content Insertion	Backdoored	49.56	34.34	58.24	77.49	81.44	62.22	60.55
	DiSP	49.22	34.80	58.17	77.10	81.44	62.88	60.60 (+0.05)
Target Refusal	Backdoored	48.44	34.39	57.87	77.36	82.04	62.48	60.43
	DiSP	49.44	33.99	57.96	77.30	80.93	62.22	60.31 (-0.12)
Misclassification	Backdoored	47.22	33.99	58.53	76.75	80.67	62.09	59.88
	DiSP	47.56	33.99	58.56	76.98	80.93	62.75	60.13 (+0.25)

## B. Implementation Details

### B.1. Overall Experimental Setup

All fine-tuning and ASR evaluation experiments are conducted on eight NVIDIA A5000 GPUs (24 GB each). During fine-tuning, we only update the projector while keeping both the vision encoder and the LLM backbone frozen. Evaluations of clean performance are carried out using the lmms-eval framework on two NVIDIA A6000 GPUs (48 GB each). For LLaDA-V, we set steps=32, gen\_length=32, and block\_length=32 when evaluating ASR. For LaViDa, we configure max\_new\_tokens=32, block\_length=32, and step\_ratio=0.5, and we disable prefix KV caching. When constructing the poisoned datasets, we replace the original responses with model-generated outputs from LLaDA-V, making the training data more consistent with the output style of MDLMs.

### B.2. Training Setting

**LLaDA-V.** We set the batch size to 32. For backdoor implantation fine-tuning, we train for 20 epochs with a peak learning rate of  $1e-4$  following a cosine decay schedule for the content insertion and targeted refusal attacks. For the misclassification attack, we train for 40 epochs with a peak learning rate of  $2e-4$ . For the corresponding DiSP defense experiments, we reduce the number of fine-tuning epochs by one order of magnitude.

**LaViDa.** For backdoor implantation fine-tuning, we set the batch size to 32 and train for 20 epochs with a peak learning rate of  $1e-4$  following a cosine decay schedule for the content insertion and targeted refusal attacks. For the misclassification attack, we set the batch size to 16 and train for 10 epochs with a peak learning rate of  $2e-4$ . For the corresponding DiSP defense experiments, we set the batch size to 32 and reduce the number of fine-tuning epochs by one order of magnitude.

## C. Results on Additional Benchmarks

To more comprehensively evaluate the impact of our method on clean performance, we extend our analysis beyond (1) MMMU [62] by incorporating five additional benchmarks spanning multiple capability axes: (2) MMLU-Pro-Standard [63], (3) MMStar [7], and (4) MMBench [39] for assessing multidisciplinary knowledge and mathematical reasoning; (5) AI2D [21] for chart and document understanding; and (6) RealWorldQA [51] for real-world scene understanding. Experimental results of LLaDA-V on these benchmarks, including the clean model (fine-tuned on clean data), the backdoored model, and the purified model after applying DiSP, are reported in Table 4. From these results, we observe that for each backdoor target, the average score over the six benchmarks exhibits only a minimal deviation after applying DiSP. The largest drop is no more than 0.12 relative to the backdoored model, indicating that our defense introduces virtually no degradation in clean performance.

## D. Visual Examples of Triggers and Poisoned Images

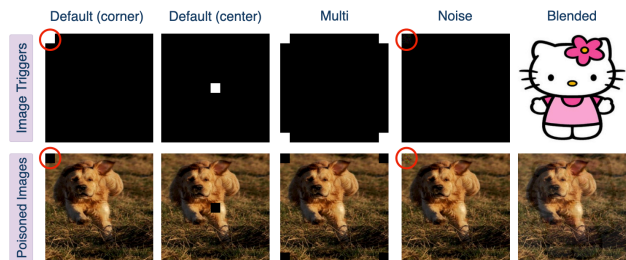


Figure 5. Illustration of triggers and poisoned images.

We provide visual examples of the triggers used in our experiments and their corresponding poisoned images in Figure 5. Specifically, we consider five representative trigger types: (1) Default (corner) [14]: inserting a  $20 \times 20$

black patch at the upper-left corner of the image. (2) Default (center): placing the same black patch at the center of the image. (3) Noise patch [40]: substituting the black patch with a Gaussian noise patch to enhance visual stealthiness (we set the standard deviation to 30). (4) Multi-trigger [45]: deploying multiple small patches within a single image to spatially disperse the trigger signal (patches are placed at all four corners in our setup). (5) Blended [8]: mixing the clean image with a target image at a fixed ratio, creating a trigger that is embedded across the entire image.